KSCE Journal of Civil Engineering (2015) 19(6):1727-1737

DOI 10.1007/s12205-015-0666-8

Highway Engineering

pISSN 1226-7988, eISSN 1976-3808
www.springer.com/12205

Microstructural Investigation of Hot Mix Asphalt (HMA) Mixtures using Digital Image Processing (DIP)

Ki Hoon Moon* and Augusto Cannone Falchetto**

Received November 6, 2013/Revised May 25, 2014/Accepted September 16, 2014/Published Online January 12, 2015

Abstract

It is well known that Nominal Maximum Aggregate Size (NMAS) significantly affects several mechanical properties of asphalt pavement layers both at low and high temperatures. Two different aggregate NMAS, 9.5 mm and 12.5 mm, are commonly used for surface layer mixture. Most of the past research studies investigated the effect of different aggregate NMAS on asphalt mixture properties through experimental testing, while the impact of NMAS on asphalt mixtures microstructure has received little attention. In this paper, asphalt mixtures with two NMAS, 9.5 mm or 12.5 mm, two air voids percentages, 4% and 7%, and two binder contents, 4% and 7%, were prepared. Then, the effect of aggregate NMAS on materials properties was investigated by performing low temperature creep test of asphalt mixture through the Bending Beam Rheometer (BBR) and advanced Digital Image Processing (DIP) analysis of two-dimensional images of asphalt mixture combined with numerical evaluations of 2- and 3- point correlation functions. As a result, asphalt mixtures containing smaller NMAS showed higher stiffness compared to those prepared with larger aggregates at low temperature. The spatial distributions of aggregates, asphalt mastic, and air voids were not significantly affected by the addition of aggregates with different NMAS. However, an increase in Auto Correlation Length (ACL) was observed for asphalt mixtures having smaller NMAS, which suggests that low temperature creep properties are associated to ACL.

Keywords: *Nominal Maximum Aggregate Size (NMAS), microstructure, Bending Beam Rheometer (BBR), Digital Image Processing (DIP), Auto Correlation Length (ACL)*

1. Introduction

Nominal Maximum Aggregate Size (NMAS) affects various mechanical properties of asphalt pavement layers both at low and high temperatures (Napa, 2001; 2009). Currently, two different NMAS, 9.5 mm or 12.5 mm, are widely used for surface layer construction in asphalt pavement. In case of base layer, aggregate with larger NMAS, 19.0 mm or 25.0 mm, are commonly used (Napa, 2001; 2009; Powell and Buchanan, 2012). Most research studies investigated the effect of using different aggregate NMAS in asphalt paving mixtures through experimental testing and performance evaluation (Napa, 2001; 2009; Buncher and Rosenberg, 2012, Powell and Buchanan, 2012).

The microstructure of asphalt mixture as described by the spatial distribution of its components, aggregate, asphalt mastic (and binder) and air voids, has received less attention, although a number of Digital Image Processing (DIP) techniques have been developed and used to model asphalt composite. Eriksen and Wegan (1993) were the first researchers to investigate asphalt binders and mixtures using DIP techniques. Yue *et al*. (1995), estimated gradation, distribution, shape and angular orientation of the aggregates skeleton using DIP analysis. Dai *et al*. (2005) coupled DIP analysis and Finite Element Method (FEM) to obtain more realistic simulation of Indirect Tensile (IDT) strength test. Kose *et al*. (2007) calculated the fraction of air void phase from 2D RGB (Red-Green-Blue) scale asphalt mixture images using DIP analysis with a fluorescent-dyed epoxy which is commonly used in ceramics research.

DIP analysis was also used to investigate the 3D distribution and interaction of aggregates, asphalt mastics (and binder) and air voids in asphalt mixtures in conjunction with 3D X-Ray Computer Tomography (CT) technology (Masad *et al*., 2002; Partl *et al*., 2007; Sefidmazgi *et al*., 2013). Recently, Zelelew *et al*. (2013) introduced advanced DIP analysis procedures and threshold algorithms for aggregate, asphalt mastic and air voids using grey scale converted asphalt mixture images. The analysis procedures are based on the input obtained through X-Ray CT technology which provides more realistic images and detailed microstructure information on asphalt mixture.

*Member, Senior Researcher, Korea Expressway Corporation, Research Institute, Corporate Strategy & Policy Research Division, Gimcheon 740-220, Korea; Korea Expressway Corporation, Research Institute Pavement Research Division, Hwaseong 445-812, Korea (E-mail: zetamkh@ex.co.kr)
**Post-Doctoral Researcher, Dept. of Architecture, Civil Engineering and Environmental Sciences - Pavement Engineering Centre (ISBS), Technical University of Braunschweig, Beethovenstraße 51 b, 38106, Braunschweig, Germany (E-mail: augcanno@tu-bs.de)

The microstructural information obtained with DIP analysis techniques can be used with high-order microstructure functions, such as *n*-point correlation functions, to compute improved upper and lower bounds of mechanical material properties (Torquato, 2000). Effective mechanical properties and failure characteristics of a heterogeneous material with the same volume fraction can be significantly influenced by the spatial distribution of its constituted particles (Torquato, 2000). In previous researches, Velasquez *et al*. (2010) used DIP analysis, a simplified gradation method and 2- and 3-point correlation functions to investigate the aggregated phase of asphalt mixture based on 2D RGB scale images. The results obtained were used as input parameters in advanced micromechanical models, and to estimate the Representative Volume Element (RVE) asphalt mixtures.

2. Research Objectives and Scopes

The main objective of this paper is to investigate the effect of adding aggregates having different NMAS(mm) on the microstructure of asphalt mixtures using 2D scanned RGB scale images of asphalt mixture and advanced DIP analyses combined with higher order microstructure functions such as 2- ad 3- point correlation functions. To accomplish this objective, the following research approach was followed:

1. Perform Bending Beam Rheometer (BBR) mixture creep test to investigate the differences in low temperature properties among asphalt mixtures having different aggregate NMAS.
2. Use digital scanning to obtain extensive information on aggregate, asphalt mastic and air voids within the asphalt mixture structure from RGB scale images of small beam specimens.
3. Obtain 2D three-phase (aggregate, asphalt mastic and air voids) asphalt mixture images using advanced DIP analysis techniques.
4. Compute the 2- and 3- point correlation functions of the aggregate, asphalt mastic and air void spatial distributions from the same 2D three-phase asphalt mixture images generated in step 3.
5. Calculate, analyze and compare the values of Auto Correlation Length (ACL) in aggregate, asphalt mastic, and air voids phases.

Table 1. Summary of Prepared Mixtures

Mixture	Group	Binder Type	Target Air void, %	NMAS, mm	*VMA*, %	V_{air}, %	V_{be}, %
1	1	PG 58-28 (Plain)	7	9.5	15.79	6.26	9.53
2			7	12.5	17.25	6.17	11.08
3			4	9.5	13.95	4.40	9.55
4			4	12.5	15.76	4.26	11.50
5	2	PG 58-28 (Modified)	7	9.5	15.85	6.53	9.32
6			7	12.5	17.09	6.04	11.05
7			4	9.5	14.77	5.14	9.63
8			4	12.5	15.40	3.93	11.47

* *VMA*: Voids in the Mineral Aggregate ($VMA = V_{air} + V_{be}$)
* V_{air} (volume of air) and V_{be} (volume of effective binder) were measured in the lab

3. Material and Testing

3.1 Sample Preparation for DIP Analysis

A set of 8 asphalt mixtures, provided from Minnesota Department of Transportation (MN/DOT), and compacted in the asphalt pavement laboratory at University of Minnesota (U of MN), were used in this study. Table 1 shows a summary of all mixtures. More detailed information can be found elsewhere (Moon, 2012).

The mixtures were prepared using two different asphalt binders (PG 58-28, Plain binder and PG 58-34, Polymer modified binder), two air void levels (4% and 7%), and two NMAS levels: 9.5 and 12.5 mm. A total of 8 asphalt mixture cylinders were prepared from Super-pave Gyratory Compactor (SGC) and five mixture slices, with the radius of 75.0 ± 10.0 mm and thickness of 12.7 ± 0.5 mm, were cut from each cylinder. Then, from each slice ten asphalt mixture beams with dimensions of 102 ± 10.0× 12.7 ± 0.5 × 6.35 ± 0.5 mm, were cut for Bending Beam Rheometer (BBR) mixture creep testing (Marasteanu *et al*., 2009; Moon, 2012) and to generate 2D three-phase asphalt mixture images.

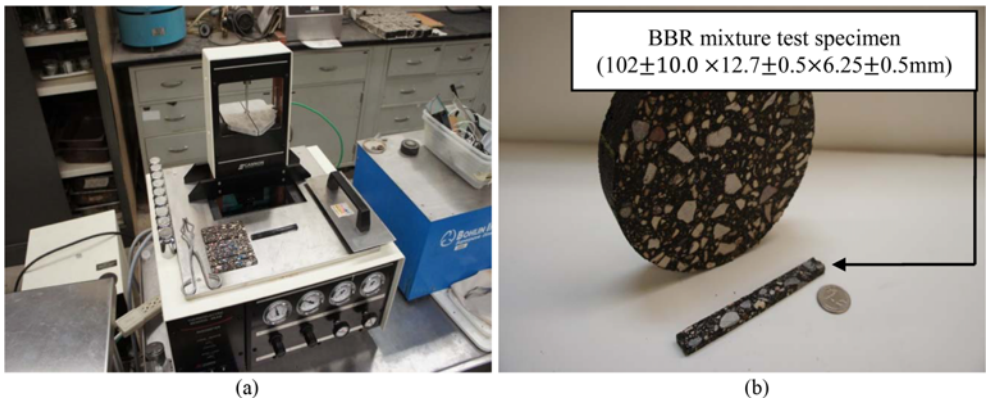

Fig. 1. BBR Mixture Test Experimental Set-up: (a) BBR Equipment, (b) BBR Testing Specimen

For DIP analysis, all beam sides (top, bottom, front and back) were scanned prior to BBR creep testing. Then, three phase asphalt mixture images containing volumetric information of aggregate, asphalt mastic and air voids were generated from 2D scanned RGB asphalt mixture beam images. In case of 2- and 3-point correlation function computation, only the top and bottom sides ($102 \pm 10.0 \times 12.7 \pm 0.5$ mm) were considered in this study. An overview on DIP analysis procedures are provided in Section 5.

3.2 Laboratory Testing

In BBR mixture creep test method, three point bending creep tests are performed on thin asphalt mixture beams using the Bending Beam Rheometer (BBR) device (AASHTO Designation T 313-06, 2006; see Fig. 1).

A constant load of 6000 g (= 6000 ± 100 mN) is instantaneously applied and maintained for 1000s, and the mid span deflection, δ(t) is measured for the entire duration of the test (Marasteanu *et al*. 2009). Low temperature creep stiffness, S(t), was calculated as:

$$S(t) = \frac{\sigma}{\varepsilon(t)} = \frac{P \cdot l^3}{4 \cdot b \cdot h^3 \cdot \delta(t)} \quad (1)$$

where, $S(t)$ is the time dependent flexural creep stiffness, MPa; σ is the maximum bending stress in the beam, MPa; $\varepsilon(t)$ is the time dependent bending strain in the beam, mm/mm; P is the constant applied load (6000 ± 100 mN); l is the length of specimen (102 ± 10.0 mm); b is the width of specimen (12.7 ± 0.5 mm); h is the height of specimen (6.35 ± 0.5 mm); $\delta(t)$ is the deflection of beam, mm; and t is the time (s).

In this research S(60s) was calculated at low PG + 10ºC for each mixture (-18ºC for PG 58-28 mixtures and -24ºC for PG 58-34 mixtures) and the values compared. A summary of BBR mixture low temperature creep testing is given in Table 2.

Table 2. Summary of BBR Mixture Creep Tests

Mixture	Binder	Temperature	Applied load (mN)
1, 2, 3, 4	PG 58-28 Plain	-18ºC (5)	6000 ± 100 mN
5, 6, 7, 8	PG 58-34 Modified	-24ºC (5)	6000 ± 100 mN

*( ): Numbers of specimen tested

4. Experimental Data Analysis

The computed results of S(60s) for each mixture based on Eq. (1) are shown in Fig.2.

As can be seen in Fig. 2, mixtures containing smaller aggregate NMAS (e.g., mixtures 1, 3 for PG 58-28 and mixtures 5, 7 for PG 58-34) showed higher low temperature creep stiffness than mixtures prepared with larger aggregate NMAS (e.g. mixtures 2, 4 for PG 58-28 and mixtures 6, 8 for PG 58-34). Moreover, stiffer mixtures are associated to lower air voids content (e.g., mixtures 1, 2(7%) vs. mixtures 3, 4(4%) and mixtures 5, 6(7%) vs. mixtures 7, 8(4%)). Two plausible explanations can be provided to interpret these results:

1. The increased particle to particle contact, present in mixtures prepared with aggregates having smaller NMAS (9.5 mm), results in higher stiffness.
2. Lower air voids contents (i.e., 4%) associated to higher compaction effort improves the stiffness properties of the mixture.

In the next section, these two hypotheses will be verified based on advanced DIP analysis and 2- and 3- point correlation functions calculation.

5. Image Analysis of Asphalt Mixtures

The internal structure of random heterogeneous materials, such as asphalt mixtures, can be studied and described using DIP analysis. A digitally converted image can be considered as a two dimensional independent function, $f(x,y)$, where f indicates the color intensity function and boundary of the image, and $f(x,y)$ represents the color intensity of the image at the specific point (x,y) (Gonzalez *et al*., 2002). The matrix representation of M×N size binary image is shown in Eq. (2):

$$f(x,y) = \begin{bmatrix} f(0,0) & f(0,1) & \cdots & f(0,N-1) \\ f(1,0) & f(1,1) & \cdots & f(1,N-1) \\ \cdots & \cdots & \cdots & \cdots \\ f(M-1,0) & f(M-1,1) & \cdots & f(M-1,N-1) \end{bmatrix} \quad (2)$$

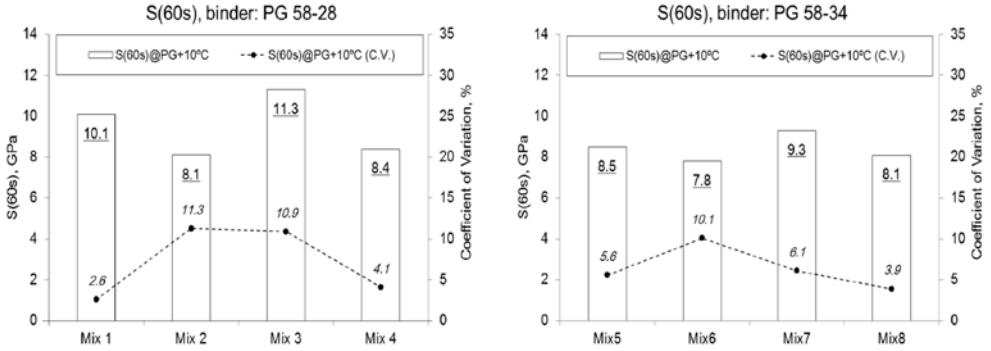

Fig. 2. S(60s) for Asphalt Mixture Testing

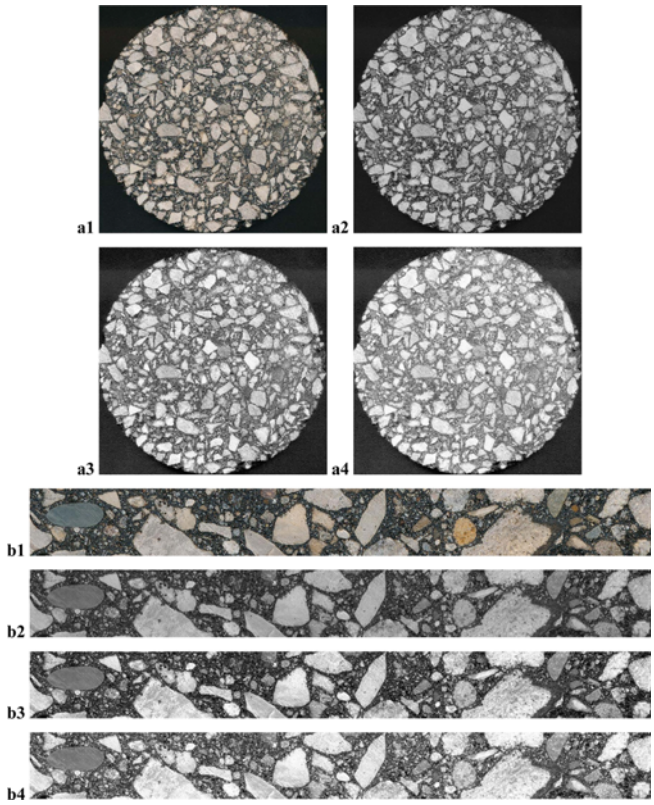

Fig. 3. DIP Analysis of Asphalt Mixture Slice (Diameter: 150 mm) and Asphalt Mixture Beam (Dimensions: 102 ± 10.0×12.7 ± 0.5 × 6.35 ± 0.5 mm): Mixture 1 [(a1) RGB Scale, (a2) Grey Scale, (a3) *histeq* Applied, (a4) *ordfilt2* Applied)] Mixture 6 [(b1) RGB Scale, (b2) Grey Scale, (b3) *histeq* Applied, (b4) *ordfilt2* Applied)]

Table 3. Summary of Computed Threshold Values, T_1 and T_2

Mixture	Group	Binder type	T_1		T_2	
			Ave	C.V.,%	Ave	C.V.,%
1	1	PG 58-28 (Plain)	92	2.05	114	1.85
2			94	4.09	126	2.05
3			85	2.27	108	0.00
4			89	2.17	121	1.59
5	2	PG 58-28 (Modified)	91	2.13	110	1.87
6			94	2.19	121	2.09
7			87	2.23	108	2.47
8			85	2.27	116	0.00

*C.V.: Coefficient of Variation (= Standard deviation/Average,%)

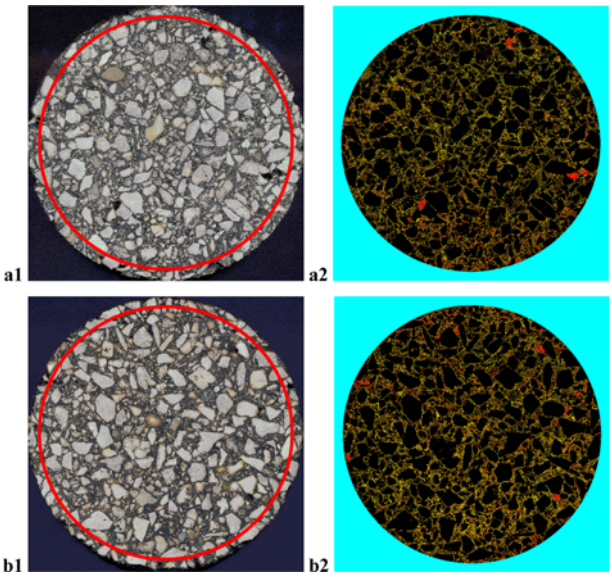

Fig. 4. 3-Phase Representation of Mixture 3 (a1~a2) and 7 (b1~b2), (Slice 1, Top): (a1) RGB Scale Image, (a2) 3-Phase (Aggregate, Mastic, Air Void) Image, (b1) RGB Scale Image, (b2) 3-Phase (Aggregate, Mastic, Air Void) Image, *Cyan color: Background, Red color: Air Void, Yellow color: Asphalt Mastic, Black: Aggregate (>75 μm), Red Circle: Portion of Image Considered for DIP Analysis

In this investigation, a flat-bed scanner was used to generate 2D images of asphalt mixture on the RGB (Red, Green and Blue) color scale. The scanning resolution used in this study was limited into 720 dpi to avoid generating and storing very large files (i.e., more than 100 MB). This resolution is sufficient to detect aggregate particles larger than 75 μm.

In previous studies (Dai *et al*., 2005; Velasquez *et al*., 2010), RGB scale asphalt mixture images were converted into binary images (black phase: air voids + asphalt binder + aggregates smaller than 75 μm, and white phase: aggregates larger than 75 μm) using different noise filtering functions. In this study, MATLAB™ Image Processing Toolbox (MATLAB, 2010) was used to convert RGB scale images of asphalt mixture into 8 bit gray scale images which contain the color intensity information in a range from 0 (black) to 255 (white). Then, three-phase asphalt mixture image, which contains aggregate, asphalt mastic (i.e., asphalt binder + aggregates smaller than 75 μm) and air voids phases, was generated using *VMA* concept. The following steps schematically describe all the DIP analysis processes performed in this research:

1) The experimentally-determined volumetric properties of the different asphalt mixtures were used to obtain the following approximated equation that was used for *VMA* calculations:

$$VMA = V_{air} + V_{be} \cong V_{air} + (V_{be} + V_{agg<75\,\mu m}) = V_{air} + V_{mastic} \quad (3)$$

where, V_{air} is the air voids fraction, V_{be} is the effective volume fraction of asphalt binder content and $V_{agg<75\,\mu m}$ is the volume fraction of aggregates smaller than 75 μm. This value is determined by the scanning resolution (720dpi) and leads to an underestimation of the effective binder, V_{be}, since it contributes to the total volume of the mastic phase (see Eq. (3)). The results of *VMA*, V_{air} and V_{be} from laboratory measurements for each mixture are shown in Table 1.

2) A set of MATLAB™ functions was next used to convert the original 80 (= 8 × 5 × 2) RGB asphalt mixture slice images to grey scale; in the meanwhile noise reduction and filtering function were further applied to improve the image quality

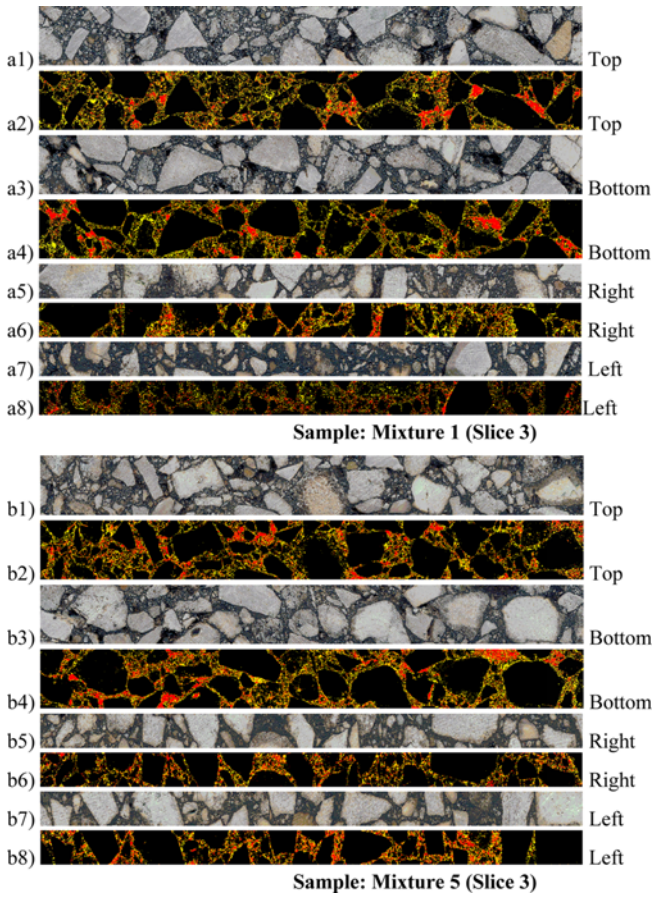

Fig. 5. Three-Phase Asphalt Mixture Beam Image, Mixture 1(a1~a8) and 5(b1~b8): (a1) RGB Image, (a2) 3-Phase Image, (a3) RGB Image, (a4) 3-Phase Image, (a5) RGB Image, (a6) 3-Phase Image, (a7) RGB Image, (a8) 3-Phase Image, (b1) RGB Image, (b2) 3-Phase Image, (b3) RGB Image, (b4) 3-Phase Image, (b5) RGB Image, (b6) 3-Phase Image, (b7) RGB Image, (b8) 3-Phase Image

(Velasquez *et al*., 2010). Then two threshold values: air void volume fraction, T_1, and mastic volume fraction, T_2, (0: black $< T_1 < T_2 <$ 255: white) were calculated from the 80 converted grey scale images of asphalt mixture slice with the assumption that the air voids phases take the darkest portion of the color intensity range (See Fig. 3). The computed values of T_1 & T_2 and generated three phase asphalt mixture slice images are shown in Table 3 and Fig. 4. In Table 3, the lower Coefficient of Variation (C.V. < 10%, max = 4.09%) values provide an indication that the scanned slices at different depth contain similar volume fractions of aggregate, asphalt mastic and air voids, however, the distribution patterns vary.

3) All the asphalt mixture slices were then cut into 400 (= 8 × 5 × 10) asphalt mixture beams having the same specimen dimensions used for BBR mixture creep test (Marasteanu *et al*., 2009) and the four sides of the samples were scanned (top, bottom, front and back), then converted into grey scale image (see Fig. 3). Finally, total 1,600 three phase asphalt mixture beam images were generated based on the T_1 and T_2 obtained in step 2. Table 4 presents the DIP results of average VMA_d, V_{air_d} and V_{mastic_d} obtained from the generated three-phase images of asphalt mixture beams. Samples of generated three-phase asphalt mixture beam images are shown in Fig. 5.

More detailed information of DIP analysis performed in this study can be referred elsewhere (Moon, 2012). The flow chart of the entire DIP analysis procedure for generating three-phase (aggregate, asphalt mastic and air void) asphalt mixture images is depicted in Fig. 6.

Based on Fig. 5, it was observed that using *VMA* for generating three phase images of asphalt mixture beams provides quite accurate and realistic three-phase images in comparison with the original RGB scale images. In addition, based on the results of Table 4, a low value of C.V. (less than 15%, max 13.00%) was found for all the analyzed mixtures. This means that each asphalt mixture beam from the same SGC asphalt mixture cylinder contains similar volume fraction of aggregates, asphalt binder and air voids in spite of the small specimen size used for the analysis.

6. Numerical Estimation of 2- and 3- point Correlation Functions

6.1 The *n*-point Correlation Function

Correlation functions provide valuable information on the reciprocal influence of different parts (i.e., phase) of a material, located at specific positions. In case of random heterogeneous

Table 4. Summary of VMA_d, V_{air_d} and V_{ma_d} for Asphalt Mixture Beam

Mix.	Group	Binder type	VMA_d, %		V_{air_d}, %		V_{mastic_d}, %		VMA^* %	V_{air}^* %	V_{mastic}^* %
			Ave	C.V.	Ave	C.V.	Ave	C.V.			
1	1	PG 58-28 (Plain)	15.79	4.99	6.26	5.98	9.52	7.44	0.16	0.17	-0.01
2			17.25	8.78	6.17	10.50	11.08	9.05	0.21	0.19	-0.40
3			13.95	2.27	4.40	5.63	9.55	3.40	0.08	0.08	-0.16
4			15.76	4.03	4.26	9.77	11.50	6.24	0.18	0.42	-0.24
5	2	PG 58-28 (Modified)	15.85	7.38	6.53	9.89	9.32	7.66	0.21	0.35	-0.14
6			17.09	8.80	6.04	7.17	11.05	9.75	0.23	0.18	-0.41
7			14.77	6.98	5.14	8.94	9.63	7.94	0.22	0.17	0.05
8			15.40	3.62	3.93	13.00	11.47	7.44	0.02	0.28	-0.26

*$VMA^* = (VMA - VMA_d)$, $V_{air}^* = (V_{air} - V_{air\_d})$, $V_{mastic}^* = (V_{be} - V_{mastic\_d})$
*Values of V_{air}, and V_{mastic}, *and VMA* can be referred from Table 1

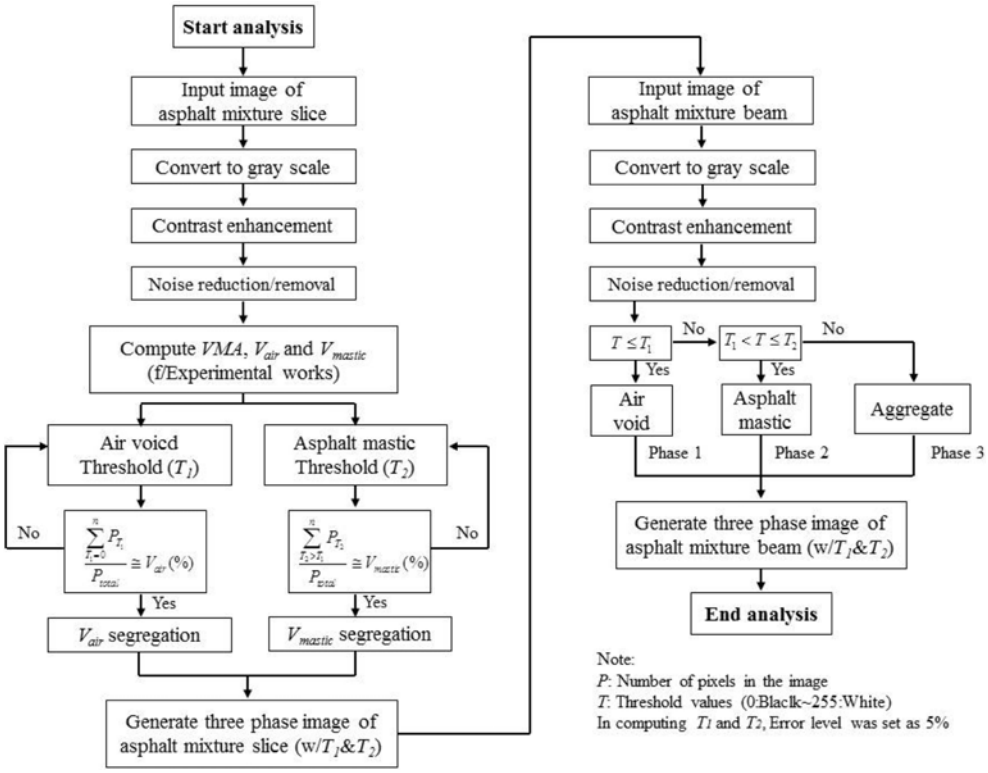

Fig. 6. Flowchart of Performed DIP Analysis in this Study

materials, higher-order microstructural information is fundamental for advanced analysis and several functions such as the *n*-point correlation functions, surface correlation functions, and lineal path functions, can be used for this purpose. Among these functions, the 2- and 3-point correlation functions are used because of their simplicity compared to the other correlation functions (Berryman, 1985; Torquato, 2002; Velasquez *et al*., 2010, Cannone Falchetto *et al*., 2013).

The *n*-point spatial correlation function calculates the probability of finding all *n* points located on the space occupied by one of the phases of a heterogeneous material (Berryman, 1985). For instance, the 1-point correlation function, S_1, calculates the probability that any point locates on phase 1, which corresponds to the volumetric fraction of phase 1. The 2-point correlation function, S_2, measures the probability that two points, separated by a certain distance, are located both in the same phase. The 3-point correlation function, S_3, computes the probability that all the vertices of a triangle are located in the same phase.

The *n*-point correlation functions of a two-phase random heterogeneous material in a *d*-dimensional Euclidian space, R^d, were defined by Torquato (2002) as:

$$S_n^{(i)}(x_1, x_2, x_3, \ldots, x_n) = \langle I^{(i)}(x_1) I^{(i)}(x_2) I^{(i)}(x_3) \ldots I^{(i)}(x_n) \rangle \quad (4)$$

where, $\langle\ \rangle$ = Ensemble averaging,
$I^{(i)}(x)$ = Indicator function defined as:

$$I^{(i)}(x) = \begin{cases} 1, & x \in V_i \\ 0, & x \in \overline{V_i} \end{cases} \quad (5)$$

$V_i \in R^d$ = Volume occupied by the i^{th} phase
$\overline{V_i} \in R^d$ = Volume occupied by the other phase.

The *n*-point correlation function shows a translationally invariant characteristic for a statistically homogeneous material and depends on the differences in the coordinate values of the x_i vectors but not on their absolute position (Torquato, 2002); this indicates that the origin of the coordinate system is not a significant factor. The *n*-point correlation function can also be formulated as:

$$S_n^{(i)}(x_1, x_2, x_3, \ldots, x_n) = S_n^{(i)}(x_{12}, x_{13}, x_{14}, \ldots, x_{1n}) \text{ for all } n \ge 1 \quad (6)$$

where, $x_{ij} = x_j - x_i$ = Difference between the two vectors x_i and x_j; and x_1 is the selected reference vector.

The 1-point correlation function represents the volume fraction ϕ_i of the selected i^{th} phase, is constant and it is the probability that a randomly selected point in the whole matrix belongs to i^{th} phase as:

$$S_1^{(i)} = \langle I^{(i)}(x) \rangle = \phi_i \quad (7)$$

The 2- and 3-point correlation function can be defined, respectively as (Torquato, 2002):

$$S_2^{(i)}(x_1, x_2) = \langle I^{(i)}(x_1) I^{(i)}(x_2) \rangle \quad (8)$$

$$S_3^{(i)}(x_1, x_2, x_3) = \langle I^{(i)}(x_1) I^{(i)}(x_2) I^{(i)}(x_3) \rangle \quad (9)$$

If the material presents a translationally invariant isotropic characteristic, the 3-point correlation function can also be written, from Eq. (8), as:

$$S_3^{(i)}(r_1, r_2) = S_3^{(i)}(|r_1|, |r_2|, u_{12}) \tag{10}$$

where, $r_1 = x_2 - x_1$ and $r_2 = x_3 - x_1$ are vectors; and u_{12} is the cosine of the angle θ_{12} between vectors r_1 and r_2:

$$u_{12} = \cos\theta_{12} = \frac{r_1 \cdot r_2}{|r_1||r_2|} \tag{11}$$

In addition, if the microstructure of the material does not present long range order, the initial value of 2- and 3-point correlation function is ϕ_i ($r = 0$); then for very large r ($r \to \infty$), they reach the asymptotic limits of ϕ_i^2 and ϕ_i^3, respectively.

$$\lim_{r\to\infty} S_2^{(i)}(r) = \phi_i^2 \tag{12}$$

$$\lim_{|r_1|,|r_2|\to\infty} S_3^{(i)}(|r_1|, |r_2|, u_{12}) = \phi_i^3 \tag{13}$$

The n-point correlation function can describe the microstructure of random heterogeneous materials such as asphalt and concrete mixtures; however, the computation process is complicated when analytical solution is used. Therefore, numerical solution is highly recommended (Torquato, 2002).

6.2 Numerical Solutions of 2-point Correlation Function

In this paper, a simplified 2-point correlation function algorithm (Velasquez *et al*., 2010) based on the Monte Carlo simulation, was used and implemented in MATLAB™ (2010) through the random number generation function, *rand*( ). Fig. 7 shows the schematic of the 2-point correlation function computation used in this research.

First, a random point, p_1, is generated. Secondly, another random point, p_2, is generated with a randomly angle θ and given length k; thirdly, the number of hits that the two randomly generated points are located in the same phase (either aggregate, asphalt mastic or air void), $N_{k\text{-}hits}$, is recorded for each k, respectively. Finally the *2*-point correlation function was computed as:

$$S_2(k, p_1, p_2) = \frac{N_{k\_hits}}{N_{total}} \tag{14}$$

In Eq. (14), N_{total} is the total number of drops at each segment length, k. Based on a previous study (Velasquez *et al*., 2010), N_{total} was set to equal to 100,000 for 2-point correlation function computations for each value of k.

To further reduce calculation time, one more condition was imposed. In the previous studies (Velasquez *et al*., 2010), the value k had a range from 0 to M/2 (= approximately 6.3 mm); however, after several computation trials the range of k was changed to 0 to M/2.5 (= approximately 5.0 mm) which reduced the computing time from 3 hours to 1~2 minutes per beam (Cannone Falchetto *et al*., 2013).

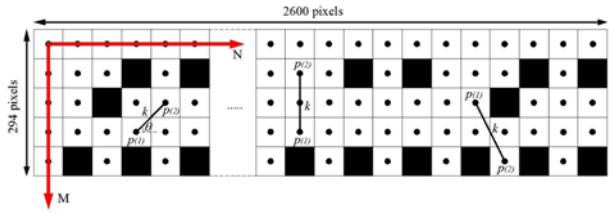

Fig. 7. Schematic of 2-point Correlation Function Computation Algorithm

Table 5. 2-point Correlation Function Values Comparison (Aggregate Phase)

Mixtures	S_1	S_2 at k = 5 mm	S_2 theoretical	Error at k = 5 mm	C.V. max
1	0.842	0.708	0.709	0.18%	3.90%
2	0.827	0.701	0.685	2.29%	5.26%
3	0.860	0.744	0.740	0.48%	3.46%
4	0.842	0.727	0.710	2.43%	2.34%
5	0.841	0.699	0.708	1.29%	3.95%
6	0.829	0.684	0.687	0.57%	3.89%
7	0.852	0.719	0.726	1.06%	3.45%
8	0.846	0.724	0.716	1.08%	4.53%

* S_1: Volume fraction of aggregate phase

In total, 15 top and bottom sides of each three-phase asphalt mixture beam images generated in section 5, which are 2600 × 294 pixels in size (102 × 12.7 mm), were randomly selected per each mixture set to perform the 2-point correlation function simulations (see Fig. 5 a2, a4, b2, b4). The summary of the 2-point correlation results for the aggregate phase is shown in Table 5. Fig. 8 presents the curves of the average 2-point function of aggregate, asphalt mastic and air voids phases for the two groups of asphalt mixtures (see Table 1).

From the computation results, all the tested mixtures showed similar behavior: the computed values of 2-point correlation function did not fluctuate with the increase of distance, k. First, it started from S_1 ($\phi_{aggregate}$, ϕ_{mastic} and $\phi_{air\text{-}void}$) and then, after increase of k, the function smoothly dropped approximately to S_1^2 ($\phi^2_{aggregate}$, ϕ^2_{mastic} and $\phi^2_{air\text{-}void}$) $\cong S_2$. This indicates that no significant differences in the random heterogeneity of the microstructure were found when using aggregate having different NMAS: 9.5 and 12.5 mm. From the results in Table 5, it was also observed that low errors (max = 2.43% for Mixture 4: aggregate phase) and C.V. (max = 5.26% for Mixture 2: aggregate phase) were detected, which indicates the stability of the computational process.

6.3 Numerical Solutions of 3-point Correlation Function

2-point correlation function can provide fundamental information about the material properties based on its microstructure. However, when clustering and/or interconnected path in the material needs to be investigated, the estimation of such higher order microstructural information can be obtained by using 3-point correlation function (Torquato, 2000). Similarly to the 2-point correlation function, the use of brute-force method, Eq. (9), is highly not recommended. To calculate 3-point correlation function, the method proposed by Velasquez *et al*. (2010), using a set of symmetric triangles based on the Monte Carlo simulation

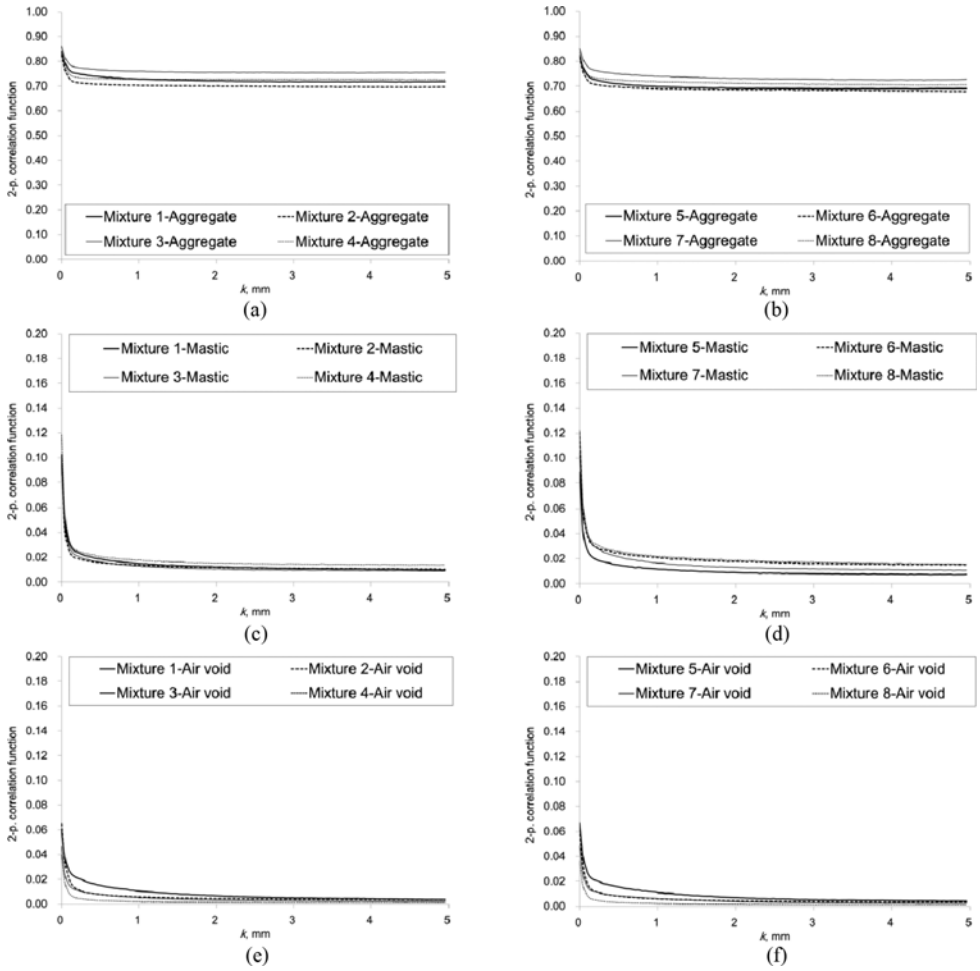

Fig. 8. 2-point Correlation Function for Mixture Groups 1 and 2: (a) Group1 (aggregate), (b) Group2 (aggregate), (c) Group1 (asphalt mastic), (d) Group2 (asphalt mastic), (e) Group1 (air-void), (f) Group2 (air-void)

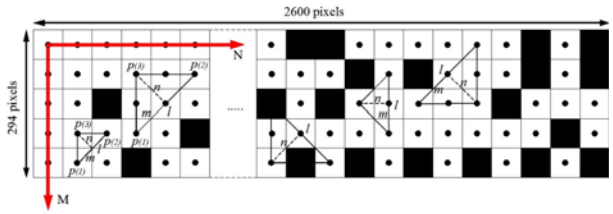

Fig. 9. Schematic of 3-point Correlation Function Computation

introduced by Berryman (1985), was used. Fig. 9 shows the schematic of 3-point correlation function computation.

For an isotropic and statistically homogeneous material, the location or orientation of a triangle does not have a significant effect, but only size and shape of triangles matters in function computation. The sets of triangle used for the calculation of 3-point correlation functions are defined by three integers: l, m and n (see Fig. 9) which are identified by the following con- straints:

$$m \le l/2 \text{ and } m^2 + n^2 \le 2\,ml \tag{15}$$

In addition, to further reduce the computation time and memory requirement during calculation, the following additional restrictions were used:

$$2m = 2n = l \text{ and } 0 \le l \le \text{int}\,(M/2.4) \tag{16}$$

In this study, symmetric triangles of the same shape but with different sizes (0 mm < l ≤ 5.2 mm) were used, which implies that the specific method selected in this study does not fully cover the entire spectrum of the 3-point correlation function; however, this is considered to have a satisfactory accuracy for the analysis purpose required in this paper while significantly reducing the computational time from 4~5 hours to 2~3 minutes per each simulation (Cannone Falchetto *et al*., 2013).

Similarly to the 2-point correlation function computation, the same 15 randomly selected top and bottom sides of generated three phase asphalt mixture images were used for each mixture set (see Fig. 5 a2, a4, b2, b4). A MATLAB^{TM} (2010) code using the random number generation function, *rand*( ), was also used for the 3-point correlation function. Each triangle defined by the integer coordinate, (*l, m, n*), was dropped in the generated 3-phase asphalt mixture image. Then, the number of hits, $N_{l\ hits}$, was counted when all the three coordinates were in the same

Table 6. 3-point Correlation Function Values Comparison (Aggregate Phase)

Mixtures	S_1	S_3 at l = 5.2 mm	S_3 theoretical	Error at l = 5.2 mm	C.V. max
1	0.842	0.606	0.597	1.44%	5.28%
2	0.827	0.592	0.567	4.24%	6.18%
3	0.860	0.653	0.637	2.41%	4.09%
4	0.842	0.623	0.598	4.02%	3.83%
5	0.841	0.606	0.596	1.69%	5.39%
6	0.829	0.573	0.570	0.50%	5.38%
7	0.852	0.636	0.619	2.71%	6.58%
8	0.846	0.629	0.606	3.76%	5.95%

aggregate, asphalt mastic or air voids phase, respectively. A total of 100,000 vector drops, N_{drops}, were used for each triangle size, l. Finally, the 3-point correlation functions for the aggregate, asphalt mastic and air-void phase were computed as:

$$S_3(l,m,n) = \frac{N_{l\_hits}}{N_{drop}} \tag{17}$$

The results of the 3-point correlation function computation for aggregate phase are listed in Table 6. Fig. 10 presents the curves of average 3-point correlation function for all four groups of asphalt mixtures of Table 1.

The computed results of 3-point correlation function did not fluctuate with the increase of l while showing low errors (max = 4.24% for Mixture 2: aggregate phase) and C.V. (max = 6.58% for Mixture 7: aggregate phase). The function starts from S_1 ($\phi_{aggregate}$, ϕ_{mastic} and $\phi_{air\text{-}void}$) and, after increase of l, smoothly drops approximately to S_1^3 ($\phi^3_{aggregate}$, ϕ^3_{mastic} and $\phi^3_{air\text{-}void}$)) $\cong S_{3,}$ similarly to the 2-point correlation function trend. Therefore, no clustering and/or connected paths (aggregate, asphalt mastic and air voids) were detected in asphalt mixtures contain aggregates having NMAS 9.5 mm and 12.5 mm, respectively.

6.4 Comparison of Auto Correlation Length (ACL)

Based on the computation results of 2- and 3-point correlation functions, Auto Correlation Length (ACL), which explains how quickly a random event decays reaches a stable value, was calculated. ACL value can also be used for estimating of Representative Volume Element (RVE) dimensions and was calculated as the length of k and l where the measured values, S_1

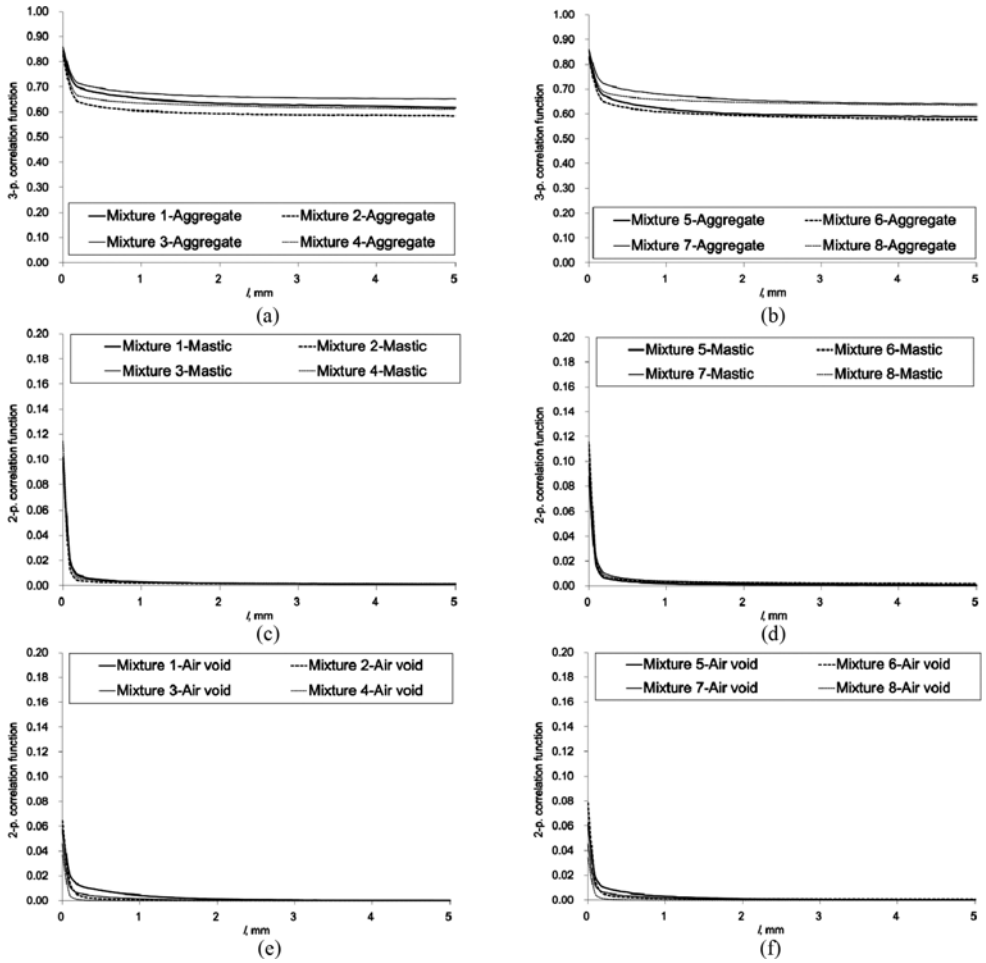

Fig. 10. 3-point Correlation Function for Mixture Groups 1 to 2: (a) Group1 (aggregate), (b) Group2 (aggregate), (c) Group1 (asphalt mastic), (d) Group2 (asphalt mastic), (e) Group1 (air-void), (f) Group2 (air-void)

Table 7. Auto Correlation Length (ACL) of 2- and 3-point Correlation Functions

(a) 2-point Correlation Function

Mixture	Binder	Group	NMAS, mm	Air v. %	ACL, mm		
					Agg.	Mas.	Air.
1	PG 58-28 (Citgo)	1	9.5	7	1.218	3.948	4.578
2			12.5	7	1.134	3.864	4.242
3			9.5	4	1.092	3.654	4.158
4			12.5	4	0.798	2.814	3.024
5	PG 58-34 (MIF)	2	9.5	7	1.176	3.906	4.452
6			12.5	7	1.008	3.696	4.032
7			9.5	4	0.966	3.486	3.738
8			12.5	4	0.672	2.646	2.856

Agg.: Aggregate, Mas.: Asphalt Mastic, Air.: Air void

(b) 3-point Correlation Function

Mixture	Binder	Group	NMAS, mm	Air v. %	ACL, mm		
					Agg.	Mas.	Air.
1	PG 58-28 (Citgo)	1	9.5	7	2.772	4.284	4.704
2			12.5	7	2.604	4.200	4.620
3			9.5	4	2.436	3.864	3.948
4			12.5	4	2.352	3.444	3.612
5	PG 58-34 (MIF)	2	9.5	7	2.604	3.948	4.620
6			12.5	7	2.520	3.780	4.536
7			9.5	4	2.352	3.612	4.116
8			12.5	4	2.100	3.276	3.528

Agg.: Aggregate, Mas.: Asphalt Mastic, Air.: Air void

approaches to their theoretical values, S^2_1 and S^3_1, respectively within 5% of error level. All the computed results of ACL are shown in Table 7.

From Table 7, it can be first observed that the values of ACL increased with respect to the three phases: aggregate, asphalt mastic and air void. This indicates larger random field and longer computational time for lower volume fraction (i.e., asphalt mastic and air voids phases) compared to the aggregate phase. Secondly, all the calculated ACL obtained on mixtures having target air voids of 4% showed smaller ACL values compared to those calculated from the 7% target air voids mixtures. This is associated to different compaction efforts used for asphalt mixture specimen preparations. Thirdly, mixtures with aggregate having NMAS = 9.5 mm showed higher values of ACL in comparison with the mixtures with NMAS=12.5 mm. This indicates larger RVE sizes need to be used when evaluating mechanical properties of asphalt mixtures contain smaller aggregate.

In section 3, stiffer characteristics at low temperature were observed in mixtures with 9.5 mm aggregate NMAS compared to mixture with 12.5 mm aggregate NMAS. Therefore it can be assumed that the increased ACL of the components of the asphalt mixture microstructure may affect low temperature creep properties based on the performed analysis. However, only eight mixtures were prepared and tested in this paper. More specimens with different combinations of asphalt binder, aggregate (type and size) should be prepared and tested to validate the findings in this research.

Moreover, it should be mentioned that even though different ACL values were observed in all the mixtures evaluated, no significant differences in microstructure and no clustering effect and/or connected paths were found for the three phases: aggregate, asphalt mastic and air void. In addition, the maximum value of ACL was 4.704 mm (Mixture 1, see Table 7b) which is smaller than the thickness (= 6.35 mm) and width (= 12.70 mm) of BBR creep mixture testing specimen.

The ACL can be used to measure the distance over which two points can be treated as independent in the specific random process (Zhang and Sundararajan, 2005). Based on this theory, other researchers (Bazant and Pang, 2007) related the Auto Correlation Length (ACL) with the estimation of the dimensions of the Representative Volume Element (RVE) of the testing material. Therefore, it can be hypothesized that BBR beam is large enough for obtaining the low temperature creep properties of asphalt mixture.

7. Conclusions

In this paper, low temperature and microstructure properties of HMA mixtures containing aggregate having different NMAS (9.5 mm and 12.5 mm) were investigated based on spatial distribution information of aggregate, asphalt mastic and air voids phases using advanced 2D DIP analysis techniques. Differently from previous studies, three-phase asphalt mixture images were generated and introduced based on *VMA* concept. It was found that these generated three-phase images can provide more realistic and accurate image of asphalt mixture which indicates this image analysis method can be potentially used also for providing advanced geometry information to FEM (Finite Element Method) and DEM (Discrete Element Method) simulation in a follow-up study.

Estimations of 2- and 3-point correlation functions were performed on the aggregate, asphalt mastic and air voids phases of the generated three-phase asphalt mixture beam images. All the 8 mixtures evaluated showed no significant fluctuations or large amount of variations in the 2- and 3-point correlation functions. No significant variation in the spatial distributions of aggregate, asphalt mastic and air voids phases were found between conventional asphalt mixtures containing two different aggregate NMAS: 9.5 mm and 12.5 mm. This is confirmed by the smooth trend of the 2-point correlation function which indicates that the observed distribution of the materials phases is typical for random heterogeneous composites. In addition the 3-point correlation function provides evidence that the microstructure does not present preferred path or clustering neither within the short range nor in the long range. However, increase of ACL was observed for mixtures containing smaller aggregate NMAS (i.e., 9.5 mm) compared to larger aggregate NMAS (i.e., 12.5 mm). This suggests there may be a correlation between ACL of asphalt mixture and low temperature creep properties since stiffer mixture showed larger ACL. In addition, based on the computed results of RVE, it can also be concluded that BBR

mixture creep test can be used as a successful testing tool for evaluating low temperature creep properties of asphalt mixture.

The images resolution used in this research does not provide an accurate estimation of the fine particles in the asphalt mixture. However, based on this advanced DIP analysis technique and on 2- and 3-point correlation functions calculations, more detailed microstructure information on asphalt mixtures can be obtained. This paper focused only on spatial distribution of aggregate, asphalt mastic and air voids in the asphalt mixture. However, in this paper, only eight mixtures were prepared and tested. More specimens with different combinations of asphalt binder, aggregate (type and size) should be considered and tested to further validate the findings in this research.

Acknowledgements

The author would like to gratefully acknowledge Mugurel I. Turos for his technical support during the experimental phase.

References

AASHTO T 313-06 (2006). *Determining the flexural creep stiffness of asphalt binder using the Bending Beam Rheometer (BBR)*, American Association of State Highway and Transportation Officials (AASHTO).

Bazant, Z. P. and Pang, S. D. (2007). "Activation energy based extreme value statistics and size effect in brittle and quasibrittle fracture." *J. Mech. Phys. Solids*, Vol. 55, Issue 1, pp. 91-134, DOI: 10.1016/j.jmps.2006.05.007.

Berryman, J. G. (1985). "Measurement of spatial correlation functions using image processing techniques." *Journal of Applied Physics*, Vol. 57, Issue 7, pp. 2374-2384, DOI: 10.1063/1.334346.

Buncher, M. S. and Rosenberg, C. (2012). *Best practice for constructing and specifying HMA longitudinal joints*, Draft Final Reports, U.S. Department of Transportation, Federal Highway Administration.

Cannone Falchetto A., Montepara, A., Tebaldi, G., and Marasteanu, M. O. (2013). "Microstructural characterization of asphalt mixtures containing recycled asphalt materials." *Journal of Materials in Civil Engineering*, ASCE, Vol. 25, No. 1, pp. 45-53, DOI: 10.1061/(ASCE)MT.1943-5533.0000544.

Dai, Q., Sadd, M., Parameswaran, V., and Shukla, A. (2005). "Prediction of damage behaviors in asphalt materials using a micromechanical finite element model and image analysis." *Journal of Engineering Mechanics*, ASCE, Vol. 131, No. 7, pp. 668-677, DOI: 10.1061/(ASCE)0733-9399(2005)131:7(668).

Eriksen, K. and Wegan, V. (1993). *Optical methods for the evaluation of asphalt concrete and polymer-modified bituminous binders,* Danish Road Institute, Note 244.

Gonzalez, R. C. (2002). *Digital image processing*, Upper Saddle River, Prentice-Hall, Woods R.E, NJ (USA).

Kose, S., Guler, M., Bahia, U. H., and Masad, E. (2007). "Distribution of strains within hot-mix asphalt binders - applying imaging and finite element techniques." *Transportation Research Record: Journal of the Transportation Board*, Vol. 1728, Issue 1, pp. 21-27, DOI: 10.3141/1728-04.

Marasteanu, M., Velasquez, R., Cannone Falchetto, A., and Zofka, A. (2009). *Development of a simple test to determine the low temperature creep compliance of asphalt mixture*, IDEA Program Final Report NCHRP 133, Transportation Research Board of the National Academies.

Masad E. Jandhyala, V., Dasgupta, N., Somadevan, N., and Shashidhar, N. (2002). "Characterization of air void distribution in asphalt mixes using X-ray computed tomography." *Journal of Materials in Civil Engineering,* ASCE, Vol. 14, No. 2, pp. 122-129, DOI: 10.1061/(ASCE)0899-1561(2002)14:2(122).

MATLAB (2010). *Help documentation*, R2010a.

Moon, K. H. (2012). *Investigation of asphalt binder and asphalt mixture low temperature properties using analogical models*, PhD Thesis, Department of Civil Engineering, University of Minnesota.

National Asphalt Pavement Association (NAPA) (2001). *HMA pavement mix type selection guide*, Federal High-Way Association and NAPA Information Series 128.

National Asphalt Pavement Association (NAPA) (2009). *Thin asphalt overlays for pavement preservation*, Federal High-Way Association and NAPA Information Series 135.

Partl, M. N., Flisch, A., and Jonsson, M. (2007). "Comparison of laboratory compaction methods using x-ray computer tomography." *Road Materials and Pavement Design*, Vol. 8, No. 2, pp. 139-164, DOI: 10.1080/14680629.2007.9690071.

Powell, R. B. and Buchanan, S. (2012). *Long term performance of a thin asphalt overlay on the NCAT pavement test track,* Transportation Research Board (TRB) 2012 Annual Meeting.

Sefidmazgi, N. R., Teymourpour, P., and Bahia, H. U. (2013). "Effect of particle mobility on aggregate formation in asphalt mixtures." *Road Materials and Pavement Design*, Vol 14, No. 2, pp. 16-34, DOI: 10.1080/14680629.2013.812844.

Torquato, S. (2000). "Modeling of physical properties of composite materials." *International Journal of Solids and Structures*, Vol. 37, Issues 1-2, pp. 411-422, DOI: 10.1016/S0020-7683(99)00103-1.

Torquatom S. (2002). *Random heterogeneous materials,* Springer-Verlag, New York.

Velasquez, R. A., Marasteanu, M. O., and Labuz, J. F. (2010). "Microstructure characterization of asphalt mixtures with 2- and 3-point correlation functions." *Road Material and Pavement Design*, Vol. 11, No. 2, pp. 251-272, DOI: 10.1080/14680629.2010.9690275.

Yue, Z., Bekking, W., and Morin, I. (1995). "Application of digital image processing to quantitative study of asphalt concrete microstructure." *Transportation Research Record: Journal of the Transportation Board*, No. 1492, pp. 53-60.

Zelelew, H. M., Almuntashri, A., Agaian, S., and Papagiannakis, A. T. (2013). "An improved image processing technique for asphalt concrete X-ray CT images." *Road Materials and Pavement Design,* Vol. 14, No. 2, pp. 341-359, DOI: 10.1080/14680629.2013.794370.

Zhang, Y. and Sandararajan, S. (2005). "The effect of autocorrelation length on the real area of contact and friction behavior of rough surfaces." *Journal of Applied Physics*, Vol. 97, Issue 10, pp. 103526-103526-7m, DOI: 10.1063/1.1914947.

http://www.trb.org/publications/pages/262.aspx,http://worldcat.org/isbn/0309061563